

AD _____

Award Number: DAMD17-00-1-0291

TITLE: A Training Program in Breast Cancer Research Using NMR
Techniques

PRINCIPAL INVESTIGATOR: Paul C. Wang, Ph.D.

CONTRACTING ORGANIZATION: Howard University
Washington, DC 20059

REPORT DATE: July 2003

TYPE OF REPORT: Annual

PREPARED FOR: U.S. Army Medical Research and Materiel Command
Fort Detrick, Maryland 21702-5012

DISTRIBUTION STATEMENT: Approved for Public Release;
Distribution Unlimited

The views, opinions and/or findings contained in this report are those of the author(s) and should not be construed as an official Department of the Army position, policy or decision unless so designated by other documentation.

20031216 133

REPORT DOCUMENTATION PAGEForm Approved
OMB No. 074-0188

Public reporting burden for this collection of information is estimated to average 1 hour per response, including the time for reviewing instructions, searching existing data sources, gathering and maintaining the data needed, and completing and reviewing this collection of information. Send comments regarding this burden estimate or any other aspect of this collection of information, including suggestions for reducing this burden to Washington Headquarters Services, Directorate for Information Operations and Reports, 1215 Jefferson Davis Highway, Suite 1204, Arlington, VA 22202-4302, and to the Office of Management and Budget, Paperwork Reduction Project (0704-0188), Washington, DC 20503

1. AGENCY USE ONLY (Leave blank)		2. REPORT DATE July 2003	3. REPORT TYPE AND DATES COVERED Annual (1 Jul 2002 - 30 Jun 2003)	
4. TITLE AND SUBTITLE A Training Program in Breast Cancer Research Using NMR Techniques			5. FUNDING NUMBERS DAMD17-00-1-0291	
6. AUTHOR(S) Paul C. Wang, Ph.D.				
7. PERFORMING ORGANIZATION NAME(S) AND ADDRESS(ES) Howard University Washington, DC 20059 E-Mail: pwang@fac.howard.edu			8. PERFORMING ORGANIZATION REPORT NUMBER	
9. SPONSORING / MONITORING AGENCY NAME(S) AND ADDRESS(ES) U.S. Army Medical Research and Materiel Command Fort Detrick, Maryland 21702-5012			10. SPONSORING / MONITORING AGENCY REPORT NUMBER	
11. SUPPLEMENTARY NOTES				
12a. DISTRIBUTION / AVAILABILITY STATEMENT Approved for Public Release; Distribution Unlimited				12b. DISTRIBUTION CODE
13. ABSTRACT (Maximum 200 Words) In the third year, this program has supported three graduate students (one from Electrical Engineering Department, one from Biochemistry Department, and one medical student) and two postdoctoral fellows (Radiology Department). The new medical student has been introduced to the Biomedical NMR Laboratory and the Howard University Cancer Center. The trainees have continued to learn the theory and instrumentation of nuclear magnetic resonance imaging and spectroscopy. The trainees have rotated through the mammography service in the Department of Radiology in the hospital to learn the mammography procedures. Besides attending weekly seminars in the Cancer Center, the trainees also have attended a special seminar series on breast imaging sponsored by this grant and the Department of Electrical Engineering. Each trainee has actively participated in one of the two research projects. Based on the experimental findings, two papers were published. Two posters have been presented in the national scientific meetings. Two graduate student trainees have received their MD or PhD degree. One graduate student received a postdoctoral award from the Army Medical Command and she will continue working as a postdoc in the Cancer Center. The PI has received a RSNA medical student departmental grant.				
14. SUBJECT TERMS Training, Nuclear Magnetic Resonance, Breast Cancer				15. NUMBER OF PAGES 30
				16. PRICE CODE
17. SECURITY CLASSIFICATION OF REPORT Unclassified	18. SECURITY CLASSIFICATION OF THIS PAGE Unclassified	19. SECURITY CLASSIFICATION OF ABSTRACT Unclassified	20. LIMITATION OF ABSTRACT Unlimited	

Table of Contents

Cover.....	1
SF 298.....	2
Table of Contents.....	3
Introduction.....	4
Body.....	4
Key Research Accomplishments.....	5
Reportable Outcomes.....	6
Conclusions.....	7
References.....	7
Appendices.....	8

I. Introduction

This is the third year of a training grant, which supports graduate students and research associates for pursuing breast cancer research using NMR techniques. There are three graduate students (Emmanuel Agwu, Lisa Kinnard and Raymond Malveaux) and two postdoctoral research associates (Ercheng Li and Renshu Zhang) supported by this grant. Emmanuel Agwu is a 7th yr MD/PhD student completing his MD program and is continuing his Ph.D. degree in Biochemistry. Lisa Kinnard is a graduate student from the Department of Electrical Engineering. She received her Ph.D. degree in June 2003. Raymond Malveaux is a second year medical student who started research in this lab at the beginning of the summer 2003. Ercheng Li is a NMR/MRI specialist. Renshu Zhang is a radiologist.

All the trainees, except Raymond Malveaux have rotated through the mammography service in the Department of Radiology to learn the mammography procedures. Besides attending the weekly seminars in the Cancer Center, the trainees also have attended a special seminar series on breast imaging sponsored by this grant and the Department of Electrical Engineering. Dr. Li and Dr. Zhang have also attended two half-day workshops at Walter Reed Hospital on small animal models for breast cancer research. Each trainee has actively participated in one of the two separate research projects. Based on the experimental findings, two papers were published. Two posters have been presented and one abstract has been submitted to three national scientific meetings. A list of the publications is included in the reportable outcomes section in this report. Lisa Kinnard has been awarded a postdoctoral grant by the US Medical Army Command. The PI has been awarded a Medical Student Departmental grant by the Radiological Society of Northern America.

II. Body

This year, we have concentrated on two research areas: (1) imaging processing techniques to separate the malignant and benign masses on digital mammograms (2) the role of P-glycoprotein modulation in drug-drug interaction.

Segmentation of Mammographic Masses Project

Mammography combined with a clinical examination is a standard method used for the detection and diagnosis of breast cancer. However, mammography alone can produce a high percentage of false positives. A computer-aided diagnostic (CAD_x) system can serve as a more accurate clinical tool for the radiologist, consequently lowering the rate of missed breast cancer and ultimately lowering morbidity and mortality. Breast cancer can exist not only in the form of masses, but also in the forms of microcalcifications, asymmetric density, and architectural distortion. These abnormalities can be seen using imaging techniques such as mammography, ultrasound and magnetic resonance imaging (MRI). Breast images have different appearances based upon their amounts of fibroglandular and fatty tissue. Fibroglandular tissue usually consists of a combination of breast glands (lobules), ducts, and surrounding fibrosis (fibrous connective tissue and scarring). It appears denser or brighter than fatty tissue on mammograms due to its higher x-ray attenuation. The diseased tissue usually also becomes denser over time. Masses can have unclear borders and are sometimes overlapped with glandular tissue in mammograms; therefore, the radiologists can overlook them during their search for suspicious

areas. Proper segmentation to include the shape and boundary characteristics is an essential step in aiding the computer for the analysis and malignancy determination of the mass. While many CAD_x systems have been developed, the development of effective image segmentation algorithms for breast masses remains unsolved in this field, particularly in the cases where the breast tissue is dense. Since cancerous masses often appear to be light and have ill-defined borders, it is quite challenging for mammographers to extract them from surrounding tissue. It is even more difficult to automatically segment masses from dense tissue. We have developed a fully automated segmentation algorithm, which delineates the complete mass as with minimum normal structures in dense and mixed tissue mammograms. The research has been summarized in three published papers listed in the appendix. An abstract, which has been submitted to an ISMRM workshop, is attached in the appendix.

P-glycoprotein Modulation Project

Cancer patients are often treated with combination therapy for secondary symptoms such as depression, and cardiopulmonary diseases. The potential for drug-drug interaction under these conditions is high. Such interactions may cause changes in the pharmacokinetics, especially for drugs with narrow therapeutic indices. These changes can alter efficacy and toxicity of the administered drugs. Drug-drug interactions may occur due to common metabolic pathways, but also due to interference at the P-glycoprotein (Pgp) level. Pgp, which is a nonspecific transport protein, is expressed constitutively at the blood-brain-barrier (BBB), intestine, kidney, liver, and in activated T-cells. Interaction at the blood-brain-barrier may occur if one of the two concomitantly administered drugs blocks Pgp thus allowing the other drug to penetrate the brain freely. The potential for drug-drug interactions is not routinely studied at the Pgp level during drug development. Its presence is assumed only after unexpected clinical symptoms. We have proposed using a dynamic NMR method based on detection of a fluorinated drug, trifluoperazine (TFP), in the brain, in combinations with an immune suppressor, cyclosporin A to demonstrate the drug penetration through the blood-brain-barrier due to Pgp modulation.

III. Key Research Accomplishments

Statement of Work: (expected in year 3)

Predoctoral Student:

- **Introduction to the Biomedical NMR Laboratory and the Cancer Center**
Raymond Malveaux was introduced to the lab and the Cancer Center. He learned the basic NMR imaging and spectroscopy techniques. He participated in the Pgp project. He is regularly attending the lab group meeting each week.
- **Report to MD/PhD committee and respective department on progress of research**
Emmanuel Agwu has reported to his PhD thesis committee twice during the year. He finished the medical school and received a MD degree. Lisa Kinnard successfully defended her PhD thesis in June 2003. She will be a postdoc at the Howard University Cancer Center.
- **Clinical preceptorship one half day per week**

Both students have rotated through the Department of Radiology Mammography Division. Lisa Kinnard also has worked with Dr. Freedman in the Department of Radiology at Georgetown University Hospital.

Postdoctoral Student:

- **Select a new research project approved by the Executive Committee**
Dr. Li and Dr. Zhang have begun working on the P-glycoprotein modulation project studying drug-drug interaction, which is an important issue for cancer therapy.
- **Clinical preceptorship one half day per week**
Dr. Li and Dr. Zhang have worked with Dr. Duckett in the Department of Radiology studying breast cancer image pattern, clinically indeterminate cases, image pattern analysis of masses vs. microcalcifications, and biopsy procedures.
- **Conduct the new research project**
The new research project: ^{19}F NMR detection of trifluoperazine crossing blood-brain-barrier through Pgp modulation.
- **Present progress report to the Executive Committee once every six months**
The progress of research was reported to the Executive Committee routinely.
- **Present research results to the Cancer Center faculty and National Meeting**
An abstract on the P-glycoprotein study has been submitted to the International Society of Magnetic Resonance in Medicine Workshop for presentation in September 2003.
- **Write scientific papers**
The trainees and PI are in the process of writing a paper entitled " ^{19}F NMR Study of Trifluoperazine Crossing Blood-Brain-Barrier Due to P-glycoprotein Modulation".

IV. Reportable Outcomes

Papers:

1. Lo S-C.B, Li H, Wang Y, Kinnard L, Freedman M, A Multiple Circular Path Convolution Neural Network System for Detection of Mammographic Masses, IEEE Transactions on Medical Imaging, Vol 21, No 2 pp 150-158. 2002 (not included in the 2002 report)
2. Kinnard L, Lo S-C B, Wang PC, Freedman MT, Chouikha M, Automatic Segmentation of Mammographic Masses Using Fuzzy Shadow and Maximum-likelihood Analysis, Proc of IEEE Symposium on Biomedical Imaging (Cat 02EX608C): pp. 241-244, 2002.
3. Kinnard L, Lo S-C.B, Wang PC, Freedman MT, Chouikha M, Separation of Malignant and Benign Masses Using Image and Segmentation Features. Proc. of SPIE, 2003 (in press)

Presentations:

1. Kinnard L, Lo S-C B, Wang PC, Freedman MT, Chouikha M. A Maximum-likelihood Automated Approach to Breast Mass Segmentation. 2002 1st IEEE International Symposium on Biomedical Imaging: Macro to Nano, Washington, DC, July 7-10, 2002.
2. Kinnard L, Lo S-C B, Wang PC, Freedman MT, Chouikha M. Likelihood Features with Circular Processing-based Neural Network for the Enhancement of Mammographic Mass

Classification. SPIE Medical Imaging Conference. San Diego, CA, February, 2003.

3. Wang PC, Aszalos A, Li E, Zhang R, Song H, A Pharmacokinetic Study of Trifluoperazine Crossing Blood-Brain-Barrier Due to P-glycoprotein Modulation. International Society of Magnetic Resonance in Medicine, Workshop on Dynamic Spectroscopy and Measurements of Physiology, Metabolism and Function. Orlando, FL, September 6-8, 2003 (submitted).

Degrees Awarded:

1. Mr. Emmanuel Agwu, an MD/PhD student, received a MD degree from the School of Medicine in June 2003. Mr. Agwu is a 3rd year PhD student in the Department of Biochemistry.
2. Ms. Lisa Kinnard received a PhD degree in June 2003 from the Department of Electrical Engineering. Her PhD thesis title is "Segmentation of Malignant and Benign Masses in Digitized Mammograms Using Region Growing Combined with Maximum-Likelihood".

Funding Applied and Received:

1. Ms. Lisa Kinnard has been awarded a Post-Doctoral Award from the US Army Medical Command entitled "Computer-Aided Detection of Mammographic Masses in Dense Breast Images"
2. Dr. Paul Wang received a Research and Education Foundation Medical Student Departmental Grant entitled "¹⁹F NMR Detection of Trifluoperazine Crossing Blood-Brain-Barrier Through Pgp Modulation" (MSD0306) from the Radiology Society of Northern America.

V. Conclusion

Lisa Kinnard has presented a new semi-automated mass segmentation scheme that combines maximum-likelihood theory with an adaptive region growing technique and area function analysis. This method has been tested on a database containing 137 mammograms of mixed visual subtlety as determined by expert radiologists. Expert radiologists have validated this segmentation scheme. It is robust and capable to distinguish the malignant masses over benign masses with reasonable confidence. This segmentation method will be incorporated into a computer-assisted mass diagnostic system to be used as a training tool for radiology residents.

The P-glycoprotein study has demonstrated that concomitantly administered a Pgp modulator enhanced TFP, an anti-psychotic drug, crossing blood-brain-barrier in vivo. It also demonstrated the pharmacokinetics of TFP accumulation in the brain. The pharmacology of this noninvasive model for realizing opening of the blood-brain-barrier in case of possible drug-drug interaction at the Pgp level was based on drug known to modulate Pgp and on the drug which can be detected by ¹⁹F NMR spectroscopy. In case of polypharmacy, like with elderly or cancer patients, drug-drug interaction is not always understood. The noninvasive dynamic NMR spectroscopy study of drug-drug interactions can be a very useful tool in drug development.

VI. References

1. Brake GM, Karssemeijer N, Segmentation of suspicious densities in digital mammograms, *Medical Physics*, 2001, vol. 28, no. 2, pp. 259-266.
2. Heath M, Bowyer KW, Kopans D et al, Current status of the Digital Database for Screening Mammography, *Digital Mammography*, Kluwer Academic Publishers, 1998, pp. 457-460.
3. Kupinski MA, Giger ML, Automated Seeded Lesion Segmentation on Digital Mammograms, *IEEE Transactions on Medical Imaging*, 1998, vol. 17, no. 4, pp. 510-517.
4. Li H, Wang Y, Liu KJR, Lo S-C, Freedman MT, Computerized Radiographic Mass Detection - Part I: Lesion Site Selection by Morphological Enhancement and Contextual Segmentation, *IEEE Transactions on Medical Imaging*, 2001, vol. 20, no. 4, pp. 289-301.
5. Li L, Zheng Y, Zhang L, Clark R, False-positive reduction in CAD mass detection using a competitive classification strategy, *Medical Physics*, 2001, Vol. 28, no. 2, pp. 250-258.
6. Mendez AJ, Tahoces PG, Lado MJ, Souto M., Vidal JJ, Computer-aided diagnosis: Automatic detection of malignant masses in digitized mammograms, *Medical Physics*, 1998, vol. 25, no. 6, pp. 957-964.
7. Petrick N, Chan H-P, Sahiner B, Wei D, An Adaptive Density-Weighted Contrast Enhancement Filter for Mammographic Breast Mass Detection, *IEEE Transactions on Medical Imaging*, 1996, vol. 15, no. 1, pp. 59-67.
8. Sahiner B, Chan HP, Wei D, Petrick N, Helvie MA, Adler DD, Goodsit MM, Image feature selection by a genetic algorithm: Application to classification of mass and normal breast tissue, *Medical Physics*, 1996, vol.23, no.10, pp.1671-1684.
9. Balis FM, Drug interaction of commonly used anticancer drugs. *Clin. Pharmacokin.*, 11, 223-235, 1986
10. Ibrahim S, Peggins J, Knapton A, Licht T, Aszalos A, Influence of beta-drenergic antagonists, H1-receptor blockers, analgesics, and quinolon antibiotics on the cellular accumulation of anticancer drug, daunorubicin: P-glycoprotein modulation. *Anticancer Res.*, 21, 847-856, 2001
11. Gottesman MM, Fojo T and Bates SE, Multidrug resistance in cancer: role of ATP-dependent transporters. *Nature Reviews*, 2, 48-58, 2002
12. Schinkel A, Wagenaar F, Mol C and Van Deemter L, P-glycoprotein in the blood-brain-barrier of mice influences the brain penetration and pharmacological activity of many drugs. *J. Clin. Invest.*, 97,2517-2524, 1996
13. Tatsura T, Naito M, Ohhara T, Sugawara I and Tsuruo T, Functional involvment of P-glycoprotein in blood-brain-barrier. *J. Biol. Chem.*, 267,20383-20391, 1992

VII. Appendices

(Three published papers and an abstract)

A Multiple Circular Path Convolution Neural Network System for Detection of Mammographic Masses

Shih-Chung B. Lo*, *Member, IEEE*, Huai Li, *Member, IEEE*, Yue Wang, *Member, IEEE*, Lisa Kinnard, and Matthew T. Freedman

Abstract—A multiple circular path convolution neural network (MCPCNN) architecture specifically designed for the analysis of tumor and tumor-like structures has been constructed. We first divided each suspected tumor area into sectors and computed the defined mass features for each sector independently. These sector features were used on the input layer and were coordinated by convolution kernels of different sizes that propagated signals to the second layer in the neural network system. The convolution kernels were trained, as required, by presenting the training cases to the neural network.

In this study, randomly selected mammograms were processed by a dual morphological enhancement technique. Radiodense areas were isolated and were delineated using a region growing algorithm. The boundary of each region of interest was then divided into 36 sectors using 36 equi-angular dividers radiated from the center of the region. A total of 144 Breast Imaging—Reporting and Data System-based features (i.e., four features per sector for 36 sectors) were computed as input values for the evaluation of this newly invented neural network system. The overall performance was 0.78–0.80 for the areas (A_z) under the receiver operating characteristic curves using the conventional feed-forward neural network in the detection of mammographic masses. The performance was markedly improved with A_z values ranging from 0.84 to 0.89 using the MCPCNN. This paper does not intend to claim the best mass detection system. Instead it reports a potentially better neural network structure for analyzing a set of the mass features defined by an investigator.

Index Terms—BI—RAD, computer-aided diagnosis, convolution neural network, mammography masses, neural network, sector features.

I. INTRODUCTION

IT IS KNOWN that effective treatment of breast cancer calls for early detection of cancerous lesions (e.g., clustered microcalcifications and masses associated with malignant cellular processes) [1]–[3]. Breast masses appear as areas of increased density on mammograms. It is particularly difficult for radiologists to detect and analyze a suspected area where a mass is overlapped with dense breast tissue. These masses are more readily seen as time progresses, but the further the tumor has progressed, the lower the possibility of a successful treatment. Therefore, increasing the chances of early breast cancer detection in improving today's clinical system is of vital importance in breast cancer diagnosis.

Several research groups have developed computer algorithms for automated detection of mammographic masses [4]–[8]. Some of these methods involved in classification of masses and normal dense breast tissues [7], [8]. Investigators also attempted to classify the malignant or benign nature of the detected tumors [9]–[11]. It is conceivable that correct segmentation of the masses [12] plays an important processing step prior to further mass analysis. In short, the results of these detection programs indicate that a high true-positive (TP) rate can be obtained at the expense of two or three false-positive (FP) detections per mammogram. Mammographically, a multiplicity (more than two) of similar benign-appearing breast lesions argues strongly for benignity [13]–[16] and, indeed, the more masses that are identified, the less chance that they represent cancer [17]. If the computer indicates multiple suspicious locations on a mammogram, the radiologist has to seek out one mass that possesses mammographic features, which are different from the others. The significant lesion may be missed due to the multiplicity of possible lesions. We, therefore, believe that a more useful and fundamental approach to computer-aided diagnosis (CAD) of masses is to devise computer programs to analyze features of a suspected area [18], [19] and to provide feature measures and estimates of the likelihood of malignancy by making comparisons within a digital mammographic database. The computer, therefore, serves as a second opinion and also provides a reproducible and an objective evaluation of the mass. With this aid, the radiologist may also increase his/her sensitivity by lowering the threshold of suspicion, while maintaining the overall specificity and reading efficiency.

Manuscript received February 22, 2000; revised January 11, 2002. This work was supported by the US Army under Grant DAMD17-96-1-6254 through a subcontract from University of Michigan, Ann Arbor, and under Grant DAMD17-01-1-0267 through a subcontract from Howard University. The work of Y. Wang was supported by the US Army under Grant DAMD17-98-1-8045. The work of L. Kinnard was supported by the US Army under Grant DAMD17-00-1-0291. The content of this paper does not necessarily reflect the position or policy of the government. The Associate Editor responsible for coordinating the review of this paper and recommending its publication was N. Karssemeijer. Asterisk indicates corresponding author.

*S.-C. B. Lo is with the Center for Imaging Science and Information System, Radiology Department, Georgetown University Medical Center, 2115 Wisconsin Avenue, Suite 603, N.W., Washington, DC 20007 USA (e-mail: lo@isis.imac.georgetown.edu).

H. Li was with the ISIS Center, Radiology Department, Georgetown University Medical Center, Washington, DC 20007 USA. He is now with the Center for Information Technology, Division of Computational Bioscience, National Institutes of Health, Bethesda, MD 20892 USA.

Y. Wang is with the Department of Electrical Engineering and Computer Sciences, The Catholic University of America, Washington, DC 20064 USA.

L. Kinnard is with the Center for Imaging Science and Information System, Radiology Department, Georgetown University Medical Center, Washington, DC 20007 USA, and also with the Department of Electrical Engineering, Howard University, Washington, DC 20059 USA.

M. T. Freedman is with the Center for Imaging Science and Information System, Radiology Department, Georgetown University Medical Center, Washington, DC 20007 USA.

Publisher Item Identifier S 0278-0062(02)02935-X.

II. CLINICAL BACKGROUND OF BREAST LESIONS AND TECHNICAL APPROACH IN MASS DETECTION

A. Description of Clinical Background

Most commonly, breast cancer presents itself as a mass. The same lesion shows a somewhat different picture from one projection to the other. Difficulties in masses also vary with the underlying breast parenchyma. In the fatty breast, masses are generally easy to detect. In the dense breast, mass detection is more difficult and auxiliary signs aid this detection. When the breast contains one mass, the decision process is based on its size, shape, and margins. When there are several masses, one looks at each, trying to determine whether any has features to suggest cancer. Furthermore, one looks to see if any mass is different in appearance from the others. Multiple small, well-defined, similar masses that present themselves bilaterally are all likely to be benign. Large, poorly defined, spiculated and unusually radiodense masses are extremely likely to be malignant. In this study, we used several computational features (see Section III-B) highly associated with four major features of breast masses routinely used in clinical reading:

- Density:** Malignant lesions tend to have greater radiographic density due to high attenuation and less compressibility of cancer than normal tissue. Radiolucent lesions are typically benign and the diagnosis can be made from the mammogram.
- Size:** If the lesion has morphological features suggesting malignancy, it should be considered suspicious regardless of the size. Isolated masses with noncystic densities greater than 8 mm in diameter can be malignant. In general, the larger a lesion, the more suspicious it is.
- Shape:** The more irregular the shape of a lesion, the more likely the possibility of malignancy. Lesions tend to be round, ovoid and/or lobulated. Small and frequent lobulations are suspicious. Lesions in the lateral aspect of the breast near the edge of the parenchyma with a reniform shape and a hilar indentation or notch usually represent a benign intramammary lymph node. Breast carcinoma hidden in the dense tissues can cause parenchymal retraction, which possess different shapes.
- Margins:** The margins of the lesion should be carefully evaluated for areas of spiculation, stellate patterns or ill-defined regions. Most breast cancers have ill-defined margins secondary to tumor infiltration and associated fibrosis. The appearance of spiculations and a more diffuse stellate pattern are almost pathognomonic for cancer. Lesions with sharply defined margins have a high likelihood of being benign; however, up to 7% of malignant lesions can be well circumscribed.

These are known clinical features and have been adapted in "Breast Imaging—Reporting and Data System" (BI—RAD) [20] of the American College of Radiology. Fig. 1(a) and (b) shows two breast images containing masses. In Fig. 1(a), a malignant mass is superimposed on the dense glandular tissue.

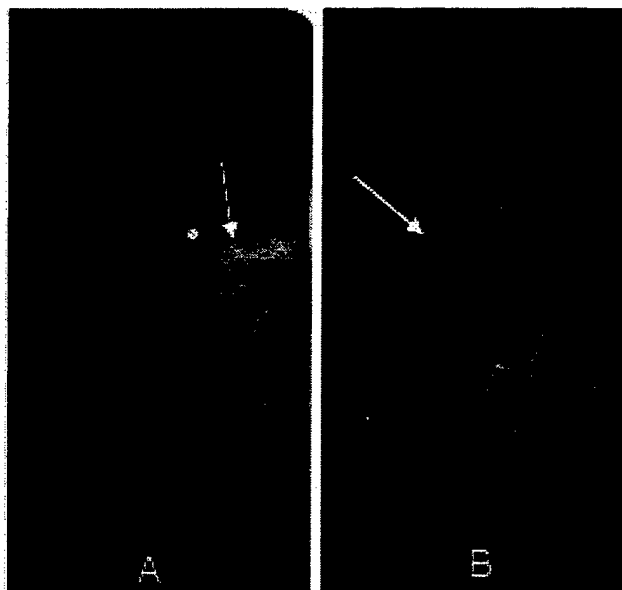


Fig. 1. (a) Dense breast containing a malignant mass. (b) Fatty and glandular breast containing a malignant mass.

However, its spiculated nature makes it easily identifiable. In Fig. 1(b), another malignant mass is located on the fatty background but is associated with a large body of glandular tissue. This mass is not easily detectable by the computer because its density is lower than the neighboring glandular tissue. Furthermore, one end of the mass is fully connected with this tissue.

B. Technical Approach for Detection of Mammographic Masses

In this study, our goal was to detect clinically suspicious lesions. The differentiation of benign and malignant status of the mammographic masses can be extended from this study model and will be reported in our future work. The study was conducted with the following steps: 1) use background correction method and morphological operations to extract radio-opaque areas; 2) delineate the boundary of the areas; 3) compute the features and texture of the masses with emphasis on the boundary; and 4) design training strategy using neural networks as classifiers for the recognition of mass features. The overall detection scheme of the study framework is shown in Fig. 2.

III. DEVELOPMENT OF TECHNICAL METHODS

A. Preprocessing and Extraction of Suspicious Masses

In automatic mass detection, accurate selection of suspected masses is considered a critical first step due to the variability of normal breast tissue and the lower contrast and ill-defined margins of masses. In our previous study [18], we aimed to improve the task of lesion site selection using model-based image processing techniques for unsupervised lesion site selection. We focused on two essential issues in the stochastic model-based image segmentation: enhancement and model selection. Based on the differential geometric characteristics of masses against

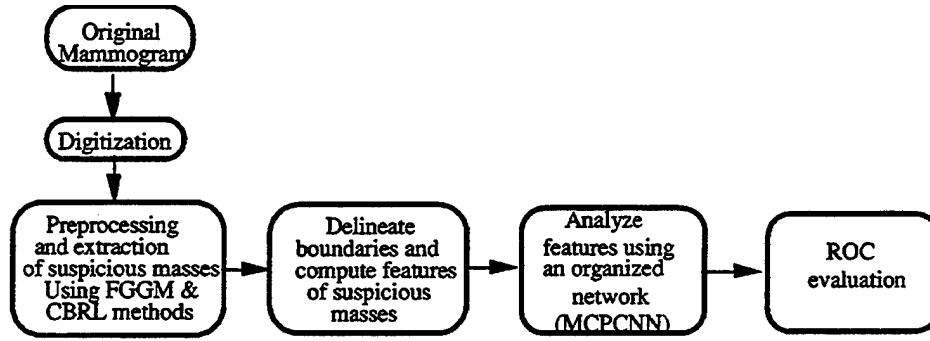


Fig. 2. A system flow chart for the detection of masses in this study.

the background tissues, we proposed one type of morphological operation to enhance the mass patterns on mammograms by removing high intensity background caused by breast tissues while maintaining mass-signals [18]. Then we employed a finite generalized Gaussian mixture (FGGM) distribution to model the histogram of the mammograms where the statistical properties of the pixel images are largely unknown and are to be incorporated. We incorporate the expectation-maximization algorithm with two information theoretic criteria to determine the optimal number of image regions and the kernel shape in the FGGM model. Finally, we applied a contextual Bayesian relaxation labeling (CBRL) technique to perform the selection of suspected masses.

We consistently processed the mammograms using this prescreening segmentation method. In the previous study [18], the FGGM method isolated 1142 potential masses including 114 of the 186 true masses in 200 mammograms. The mammograms were collected from the Mammographic Image Analysis Society (MIAS) database [21] and Brook Army Medical Center (BAMC) database. After morphological enhancement, 3143 potential masses were extracted using the FGGM technique. Of them, 181 were masses; however, five masses were not extracted. The results demonstrated that more true masses were picked up after enhancement although more false cases were also included. The undetected areas mainly occurred at the lower intensity side of the shaded objects or more obscured by fibroglandular tissues that, however, were extracted on morphological enhanced mammograms. Additionally, when the margins of masses are ill defined, only parts of suspicious masses were extracted from the original mammograms. We, therefore, decided to use the proposed morphological operation as a preprocessing step for the image enhancement prior to a segmentation method for the extraction of potential masses on the mammograms.

Based on the CBRL segmented region of interest (ROI), we employed a region growing method using a four-neighbors connection method assisted with a template masking operation to fill unconnected holes in the ROI

$$\text{IF } f(x-a, y-b) > V \text{ and } f(x, y) \in S, \\ \text{then } f(x-a, y-b) \in S \quad (1)$$

$$\text{IF } f(x-d, y-d) \in S, \text{ then } f(x-t, y-s) \in S \\ \text{for } t \leq d \text{ and } s \leq d \quad (2)$$

where V denotes the threshold value of the originally CBRL segmented ROI, S represents the set of growing region, and $[a, b]$ is a set of four conditions (i.e., $[1, 0]$, $[-1, 0]$, $[0, 1]$, and $[0, -1]$) for the four neighboring pixels. In (2), d is the size of template. In practice, we found that d should be set at five pixels to fill the holes without disrupting the boundary.

B. Feature Extraction of the Masses

Feature extraction methods play an essential role in many pattern recognition tasks. Once the features associated with an image pattern are extracted accurately, they can be used to distinguish one class of patterns from the others. Recently, many investigators have found that the multilayer perceptron (MLP) neural network using the error backpropagation training technique is a very powerful tool to serve as a classifier [22], [23]. In fact, the use of MLP neural network system for classification of disease patterns has been widely applied in the field of CAD [24]–[28].

The success of using a classifier for a pattern recognition task would rely on two factors: 1) selected features that could describe a discrepancy between image patterns and 2) accuracy of the feature computation. Should either one fail, no analyzer or classifier would be able to achieve an expected performance. By analyzing many clinical samples of various sizes of masses, we found that the peripheral portion of the mass plays an important role for mammographers to make a diagnosis. The mammographer usually evaluates the surrounding background of a radio-dense area when a region is suspected.

We used the CBRL segmented ROI to compute the center. Since the segmented ROIs were somewhat smaller than the mammographer's delineation and on the denser region of the suspected patch, the computed centers were quite close to the visual center. We then divided the boundary of the ROI into 36 sectors (i.e., 10° per sector) using 36 equi-angular dividers radiated from the center of the ROI. The following features were computed within each 10° sector of the region.

- " l "—the length from the center of the ROI to the boundary segment of the sector.
- " a "—the $\cos(\theta)$ (where θ is the normal angle of the boundary).
- " g "—the average gradient of gray value on the segment along the radial direction (i.e., $g = \sum_{i=1}^N \{g_i/N\}$) where N is the number of pixels of i along the radial direction from $l/3$ inside the boundary to the boundary (see the left

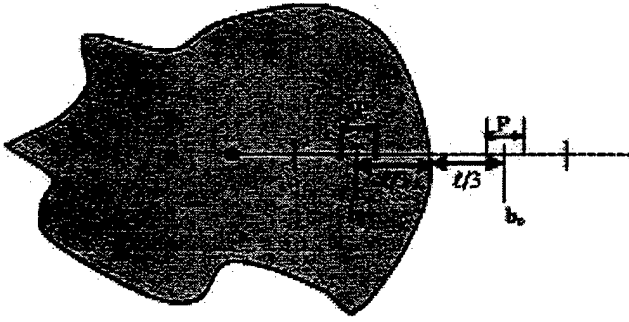


Fig. 3. A suspicious mass is delineated and shown as the shaded region. Contrast is computed by subtracting the average background pixel value (i.e., b_o , $o = 1, 2, \dots, P$) from the average foreground value (i.e., h_i , $i = 1, 2, \dots, P$).

$l/3$ line segment, Fig. 3). Technically speaking, this set of gradient values may also serve as a fuzzy system on the input layer in the neural network (to be described in Section III-C).

- d) "c"—the gray value difference (i.e., contrast) along the radial direction. Specifically, $c = \sum_{i=1}^P \{h_i/P\} - \sum_{o=1}^P \{b_o/P\}$ where h_i (or b_o) represents a pixel value along the radial direction. The position $l/3$ inside the boundary is the center of pixels h_i ($i = 1, 2, 3, \dots, P$) and position $l/3$ outside the boundary is the center of pixels b_o ($o = 1, 2, 3, \dots, P$), and P is the number of pixels equivalent to a segment of $l/6$ and was used for averaging (see Fig. 3).

Hence, a total of 144 computed features (four features/sector for 36 sectors) were used as input values for the classification of the ROI. The relationship between the computed features and BI—RADS descriptors are discussed below.

- i) ROI Size—The size of ROI is provided by the 36 "l" values.
- ii) ROI Shape (round, oval, lobulated, or irregular)—The 36 "l" and 36 "a" values can describe the shape of the ROI.
- iii) ROI Margin (circumscribed, microlobulated, obscured, ill-defined, or spiculate)—The 36 "g" and 36 "l" values can describe the ROI margin.
- iv) ROI Density (fat-containing, low density, isodense, or highly dense)—The 36 "c" and 36 "g" values can be used to describe the density distribution of the ROI.

In short, the selected features are greatly associated with the main mass descriptors indicated in the BI—RADS. The reason for using 36 values for each nominated feature is four-fold: 1) mass boundary varies, it is difficult to describe an image pattern using a single value; 2) due to the general shape of the masses, the features of masses can be easily analyzed by the polar coordinate system; 3) in case some features are inaccurately computed in several directions due to the structure noises, such as the breast slender lines, there may still exist a sufficient number of correct features; and 4) generally more accurate results can be produced by using subdivided parameters rather than using global parameters in a pattern recognition task when the parameters are barely discernable and sample sizes are sufficiently large. Other computational features (e.g., difference

entropy [19] and other higher order features) are eligible but require further investigation.

C. The Neural Network Structure Specifically Designed for the Extracted Boundary Features

1) *Multiple Paths With Circular Networking to Instruct the Neural Network in Analyzing Sector Features*: This paper focuses on neural network design and arrangement of features for effective pattern recognition of ROIs. We designed several neural network connections between the input and the first hidden layers as shown in Fig. 4. In this neural network system, the first layer also functions as a correlation layer that transforms and encodes the signals from input nodes into correlation features for further neural network process. Fig. 4(a)–(c) illustrates the full connection (FC), a self correlation (SC) network, and a neighborhood correlation (NC) network, respectively. Network connections with multiple sectors (i.e., 20° , 30° , 40° , and 50° of the NC) are grouped separately as independent NC paths. In the following study, we used four SC paths for a single sector and thirteen NC paths for four types of multisectors. The method of using the multiple correlation connections was motivated by our research experience in two-dimensional (2-D) convolution neural network (CNN) [(2-D CNN)] where we found that more than ten multiple convolution kernels in the CNN were necessary in the detection of lung nodules and microcalcifications [25].

Compared with 2-D CNN systems, the computation required in the one-dimensional (1-D) CNN (e.g., 144 input features) is relatively small. The combination of the networking paths described earlier for multiple circular path convolution neural network (MCPCNN) was implemented using C programming language. The internal computation algorithm used in the MCPCNN shares the same convolution process as that in the 2-D CNN [25]. Rotation invariance and flip invariance for training the 1-D convolution kernels in the MCPCNN were employed.

The fully connected neural network is a conventional feed-forward MLP neural network. The signals of the fully connected neural network join the other network processes (i.e., SC paths and NC paths) at the single node of the output layer. The signal received at the output node is scaled between zero and one. During the training, zero and one were assigned at the output node to perform backpropagation computation for a nonmass and a mass, respectively. The backpropagation is computed in such a way that the computed incremental errors [see equations (9) and (10)] are retraced into every independent network path. Excluding the output layer, the SC and NC signals are independently arranged and are processed through the 1-D convolution process in the forward propagation. The learning algorithms for all three types of circular network paths are based on the backpropagation training method.

Let $V^0(n', s')$ represents an input signal at the node n' and sector s' . The signal processed through an NC path and to be received at each node, n , on the first hidden layer is

$$N_{j[NC]}^1(n) = \left[\sum_{s'} \sum_{n'} V^0(n', s') \cdot W_{j[NC]}(n', s'; n) \right] + b_{j[NC]}^0(n) \quad (3)$$

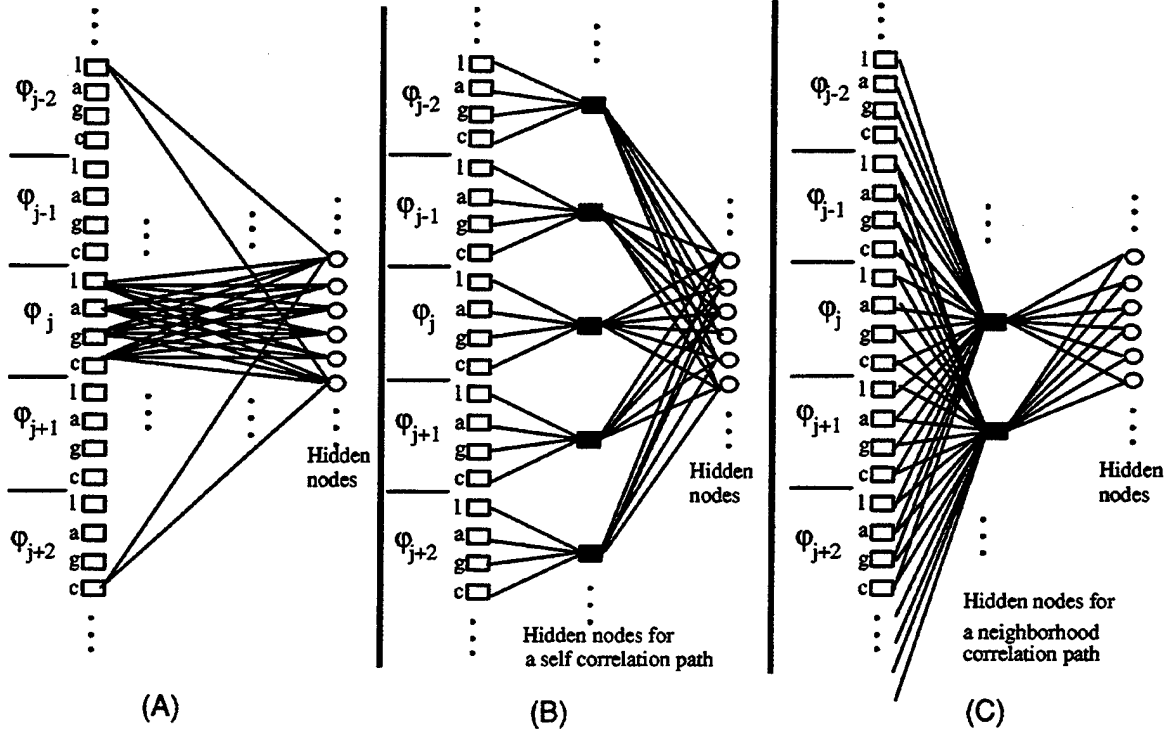


Fig. 4. Three types of network paths connecting the input and the hidden layers in the MCPCNN. (a) FC path. (b) SC path. Each node on the layer connects to a single set of the features (l, a, g, c) for the fan-in and fully connects to the hidden nodes for fan-out. (c) A NC path. Each node on the layer connects to the input nodes of adjacent sectors for the fan-in and fully connects to the hidden nodes for fan-out. The fan-in nets emphasizing SC in (b) and NC in (c) represent convolution weights (i.e., the same type of sectors possess the same set of weighting factors).

where $b_{j[NC]}^0(n)$ represents the bias term and $W_{j[NC]}(n', s'; n)$ is an array associated the 2-D nets that fan-in to a given receiving node, n . Each element of $W_{j[NC]}(n', s'; n)$ is the weight factor connected to node n from node n' sector s' through a NC path, j , and s' covers a range of neighborhood sectors corresponding to each type of NC path. Note that multiplications between the input nodes and connecting weights are computed first followed by taking the sum of the products for those nodes and sectors involved. The operation is repeated by shifting the weights from one set of sectors to the next. The procedure involving array multiplication passing through every sector is referred as the 1-D convolution operation that takes place in the sector dimension. The signal processed through an SC path and to be received at a node, n , on the first hidden layer is a special case of an NC path when s' only covers one sector

$$N_{i[SC]}^1(n) = \left[\sum_{n'} V^0(n', s') \cdot W_{i[SC]}(n'; n) \right] + b_{i[SC]}^0(n) \quad (4)$$

where $W_{i[SC]}(n'; n)$ is the weight factor connected to n from node n' through a SC path, i , regardless of the sectors. A total of 18 paths (1 FC, 4 SC paths, and 13 NC paths for four types of multisectors) were used in our experiment described later. Nevertheless, the signals processed through a path and to be received at each node, n , on the first hidden layer is

$$V_P^1(n) = S(N_P^1(n)) \quad (5)$$

where p is one of the network paths and $S(z)$ is a sigmoid function given by

$$S(z) = \frac{1}{1 + \exp(-z)}. \quad (6)$$

The sigmoid function would produce modulated values ranging from zero to one. The signals on other hidden layers in each path are processed the same as a conventional fully connected neural network. Other than the first hidden layer, the receiving signals at a hidden layer, l , collected from the previous hidden layer, $l-1$ to one, are merged from the nodes in the last layer and are given by

$$V^l(n) = S(N^l(n)) \\ = S \left(\sum_{n'} V^{l-1}(n') \cdot W^{l-1}(n'; n) + b^{l-1}(n) \right) \quad (7)$$

where n' and n denote the nodes at layers $l-1$ and l , respectively.

Let the t th change of the weight be $\Delta W_P^t(n', s'; n)$ and the t th change of the bias be $\Delta b^t(t)$. The error function is defined as

$$E = \frac{1}{2} (T - O)^2 \quad (8)$$

where T and O denote the target output value and the actual output value, respectively when the input values $V^0(n', s')$, are

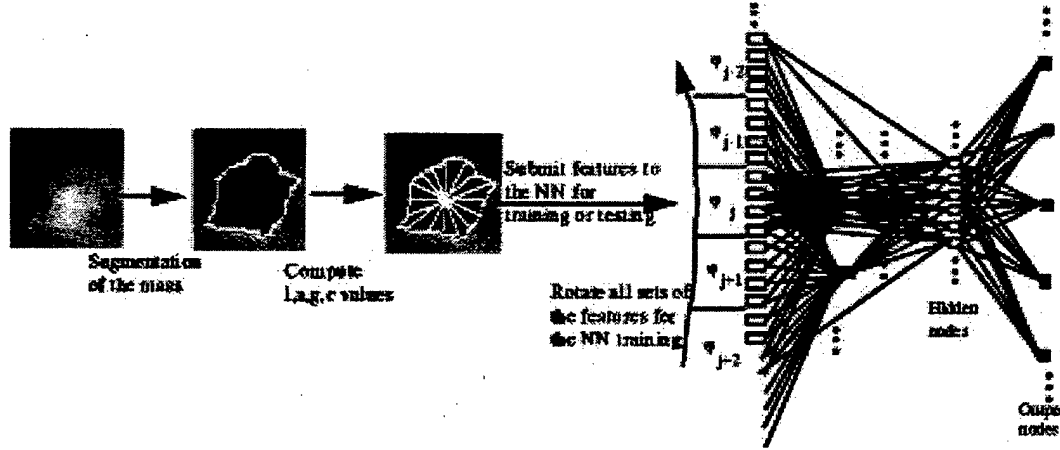


Fig. 5. A schematic diagram, showing the MCPCNN and sector features of masses, that was used in the following study.

entered in the network. In this model, the error backpropagation algorithm, which updates the kernel weights, is given below

$$\begin{aligned} \Delta W_p^l[t+1] &= \eta \left(\sum_n \sum_s \delta_p^{l+1}(n', s'; n, s) \cdot V_p^{l+1}(n, s) \right) \\ &\quad + \alpha \Delta W_p^l[t] \end{aligned} \quad (9)$$

$$\Delta b_p^l[t+1] = \eta \sum_n \sum_s \delta_p^{l+1}(n', s'; n, s) + \alpha \Delta b_p^l[t] \quad (10)$$

$$\begin{aligned} \delta_p^l(n', s'; n, s) &= S'(N_p^l(n', s')) \left(\sum_n \sum_s \delta_p^{l+1}(n, s) \cdot W_p^{l+1}(n, s) \right). \end{aligned} \quad (11)$$

In the case of the last layer

$$\delta^L(n) = S'(N^L(n)) (T(n) - O(n)) \quad (12)$$

where $S'(z)$, η , α , and T denote the derivative of $S(z)$, the learning rate, the weighting factor contributed by the momentum term, and the desired output image, respectively. Furthermore, s or $s' = 1$ and $p = 1$ when $l \neq 0$.

During the training, we added an isotropic constraint to the weights of the 1-D convolution kernels so that

$$W_q^0(n, -s) = W_q^0(n, s) \quad (13)$$

where q is not the fully connected path. These additional constraints are used to induce the kernels functioning as correlation processing filters and could facilitate the algorithm in searching for an appropriate filter.

2) *Resampling the Training Set Through Utilization of Rotation and Flip Invariance of the Features:* In this neural network model, there are no starting and ending sectors. The forward and backpropagation computation can start from any sector. Considering a flipped patch, the characteristics of mass feature should remain the same. To take advantage of this flip invariance, the same numerical target value can be assigned at the output node

for the flipped image patch in order to double the amount of cases during training.

Since we designed a 10° increment for each rotation, every SC or NC path would process through 36 times using the defined features for each image patch. To simplify this network computation, we shifted one small sector (four nodes) on the input layer at a time to conduct the circular convolution process with the SC and NC kernels in the following experiments. By reversing the sequence of the sector, one can train the flipped version of the suspicious masses. Hence, using the properties of the rotation invariance and flip invariance for the neural network training literally increases the number of the training set by a factor of 72.

In summary, we have developed a complete detection procedure for the automatic recognition of mammographic masses including background adjustment, contrast enhancement, ROI segmentation, feature extraction, and MCPCNN system with a training method. Fig. 5 shows a flow diagram for the essential sections of the computational procedures.

IV. EXPERIMENTS AND RESULTS

As described in Section III-A, the 200 mammograms were selected from the MIAS database and the BAMC database for the study. Of the 200 mammograms, 50 mammograms are normal, and each of the 150 abnormal mammograms contains at least one mass case of varying size, subtlety, and location. Both the cranio-caudal (CC) and medio-lateral oblique (MLO) projection views were used. The films were digitized with a computer format of $2048 \times 2500 \times 12$ bits (for an $8'' \times 10''$ area where each image pixel represents $100 \mu\text{m}$ square). Ninety-one mammograms, either a CC or an MLO view film, were selected from 91 patient film jackets. No two mammograms were selected from the same patient. All the digitized mammograms were miniaturized to $512 \times 625 \times 12$ bits using 4×4 pixel averaging before the method was applied. According to radiologists, the size of small masses is 3–15 mm in effective diameter. A 3-mm object in an original mammogram occupies 30 pixels in a digitized image with a $100\text{-}\mu\text{m}$ resolution. After reducing the image size by four times, the object will occupy the range of about 7–8 pixels. The object with the size of seven pixels

is expected to be detectable by any computer algorithm. After preprocessing and an object screening based on the circularity test and the size test (between 3 and 30 mm), a total of 125 suspicious areas were selected from the testing mammograms (91 cases) for this study. Specifically, the screening procedure of reducing FPs involves two steps: 1) image patches with circularity less than 0.25 or diameter greater than 30 mm were eliminated and 2) using probability modular neural network to rule out the majority of FPs. Of the 125 suspicious areas, 75 ROIs contained masses based on corresponding biopsy reports with one experienced radiologist reading. Of 75 masses, 39 were malignant and 36 were benign. This set of ROIs was used in [19] and discussed in [19, Fig. 6 and Table II].

A. Experiment 1

Of the 125 suspicious areas, we randomly selected 54 computer-segmented ROIs where 30 patches were matched with the radiologist's mass identification and 24 were not. This database was used to train two neural network systems: 1) a conventional three-layer neural network and 2) the proposed MCPCNN training method using the same neural network learning algorithm. The structure of the MCPCNN was described earlier. In the study, we used one fully connected path, four SC paths, four NC paths covering two sectors, four NC paths covering three sectors, three NC paths covering four sectors, and two NC paths covering five sectors in the first step network connection for the MCPCNN. All paths in the neural network have their hidden layers. Only one hidden layer per path was used. Both neural network systems were trained by the error backpropagation algorithm by feeding the features from the input layer and registering the corresponding target value at the output node. Completion of the training was determined by the mean square error [i.e., $\sum_{i=1}^N (T_i - O_i)^2 / N$, where N is number of samples] when it was approximately reduced to 3×10^{-5} . Once the training of the neural networks was completed, we then used the remaining 71 computer segmented ROIs for the testing. Forty-five out of 71 ROIs were masses and 26 ROIs were not. Neither the images nor their corresponding patients in the testing set could be found in the training set. The neural network output values were fed into the LABROC4 program [29] for the performance evaluation. The results indicated that the areas (A_z) under the receiver operating characteristic (ROC) curves were 0.7869 ± 0.0536 and 0.8443 ± 0.0457 using the conventional neural network (MLP) and the MCPCNN, respectively. The ROC curves of these two neural network systems are shown in Fig. 6(a). The A_z value was 0.7869 ± 0.0536 when using the MLP method with 125 hidden nodes. The performance of the MLP remains about the same at 0.7809 ± 0.0551 of A_z using the same neural network parameters but with 30 hidden nodes.

We also invited another senior mammographer to conduct an observer study using the ROC study protocol. The mammographer was asked to rate each patch using a numerical scale ranging from zero to ten for its likelihood of being a breast mass. The image patches were displayed on a SUN monitor (Model: GDM-20D10). The image size shown on the monitor was reduced to approximately $7'' \times 9''$ as compared with the original film size ($8'' \times 10''$). These 71 numbers were also fed into the LABROC4 program. The A_z of the mammographer's perfor-

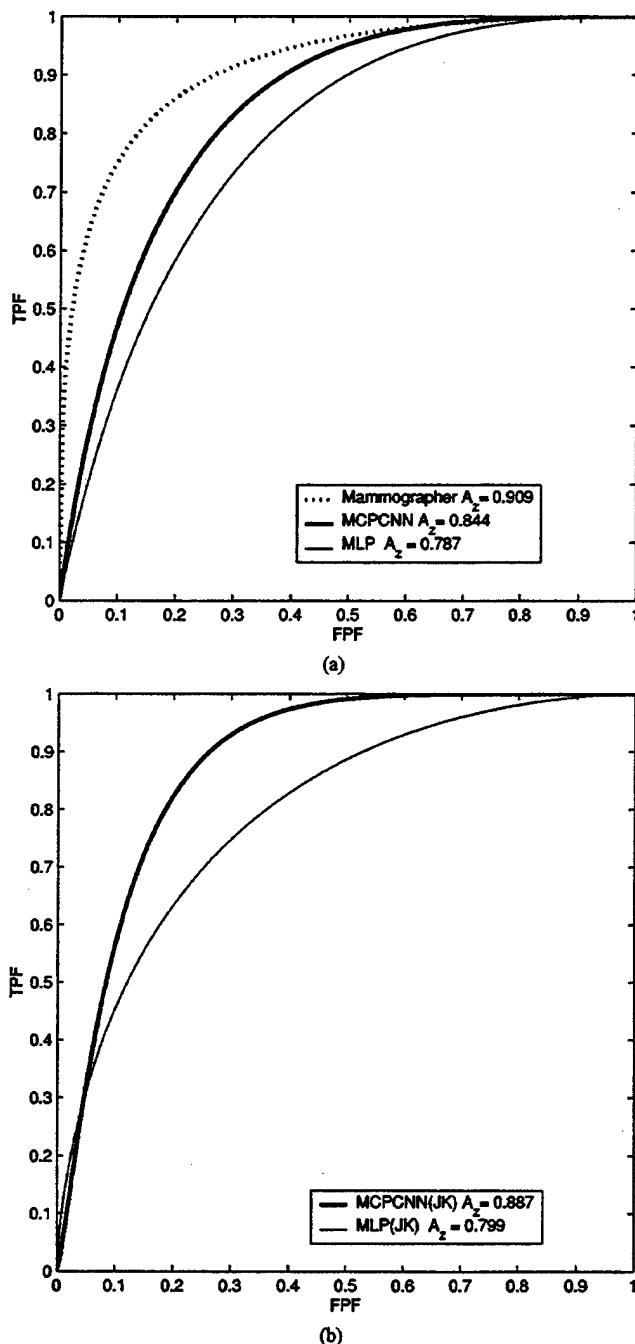


Fig. 6. The ROC curves obtained from corresponding experiments. (a) Shows that the performance of MCPCNN training method is superior to that of the conventional MLP method. The highest curve is the ROC performance of the senior mammographer. (b) Shows that the ROC results were increased using the leave-one-case-out procedure in both neural network systems. The MCPCNN still showed higher performance than conventional MLP method.

mance on this set of test cases was 0.909 ± 0.0340 . The corresponding ROC curve is also shown in Fig. 6(a).

B. Experiment 2

We also conducted a leave-one-case-out experiment (i.e., jackknife procedure) using the same database. In this experiment, we used those image patches extracted from 90

TABLE I
ROC PERFORMANCE OF THE TEST METHODS IN DISTINGUISHING TRUE AND FALSE MASSES

	Comparative Analyses of Methods	A_z of Method (1)	A_z of Method (2)	P Values	Statistical Significance
Experiment 1	(1) Radiologist vs. (2) MCPCNN	0.909 ± 0.0340	0.8443 ± 0.0457	0.1855	No
	(1) Radiologist vs. (2) MLP	0.909 ± 0.0340	0.7869 ± 0.0536	0.0447	Yes
	(1) MCPCNN vs. (2) MLP	0.8443 ± 0.0457	0.7869 ± 0.0536	0.1344	No
Experiment 2	(1) MCPCNN vs. (2) MLP	0.8866 ± 0.0289	0.7985 ± 0.0394	0.0241	Yes

mammograms (one mammogram per case) for the training and used the image patches (most of them are single) extracted from the remaining one mammogram as test objects. The procedure was repeated 91 times to allow every ROI extracted from each mammogram to be tested in the experiment. For each individual ROI, the computed features were identical to those used in Experiment 1. Again, the training was stopped when the mean square error value approximately equal to 3×10^{-5} . Both neural network systems were independently trained and evaluated with the same procedure. The results indicated that the A_z values were 0.7985 ± 0.0394 and 0.8866 ± 0.0289 using the conventional neural network (MLP) and the MCPCNN, respectively. The performance of the MLP decreased to an A_z of 0.7608 ± 0.0429 using the same neural network parameters but with 30 hidden nodes. Fig. 6(b) shows the ROC curves of these two neural network systems using the leave-one-case-out procedure [30] in the experiment.

We also used CLABROC program [31] to analyze the ROC data and compare the ROC results. The results and their statistical significances using two tailed p value of 0.05 as the threshold are shown in Table I. The radiologist's performance is greater than conventional neural network system with a p value of 0.0447 in the first experiment. The MCPCNN was also proven to be superior to the MLP with a statistically significant result ($p = 0.0241$).

V. DISCUSSION

It is known in the field of artificial intelligence that the key factors in pattern recognition are: 1) effective methods in the extraction of features and 2) classification methods for the extracted features. In this study, we showed that the training method designed to guide the analyzer is also an important factor for a pattern recognition task. Though this finding is not new, the research of developing training methods for various pattern recognition tasks has not been established in the field of medical imaging. Our studies demonstrated that with proper network connections and task-oriented guidance, organized features would assist the neural network in performing the task.

Technically speaking, a feed-forward MLP neural network provides an integrated process for classification and sometimes for feature extraction. The output values of the hidden nodes can be interpreted as a reorganized set of features presented to the output layer for classification. The drawback of the MLP is, the user has a very little control and little understanding about the network learning. The MCPCNN is a network design that partially remedies these issues and is applicable for any pattern recognition task associated with ROIs. The MCPCNN (a

member of the CNN family) possesses shared weights in the hidden layer(s) that act as filter kernels for extracting correlated features. With a higher resolution mammogram, a finer sector ($<10^\circ$) would be preferred for the analysis mass, especially for the study of classification of masses. During forward and back-propagation training, the kernels would comply with both signals from input and output layers for all training cases, so as to maximize the classification performance. We do not recommend using 2D CNN for the detection of masses because the mass sizes vary from a few millimeters to 4 cm or even larger. It would require a large fixed size to cover the maximum mass size when using the 2-D CNN. The varieties of mass shapes and potential long spiculated patterns make the use of the 2-D CNN not practical. Since the MCPCNN processes the features computed from sectors, it does not limit the sizes of its ROIs. Best of all, the MCPCNN also has the ability to classify partially obscured masses. The 2-D CNN, however, would be more appropriate for the detection of microcalcifications and small lung nodules.

As far as the research in the detection of masses is concerned, we have shown that use of MCPCNN with sector features is an effective approach. Since the MCPCNN coordinates the input data and performs correlation between features of adjacent sectors in the first stage of data processing, the internal neural network learning algorithm can be changed if a learning algorithm is found to be more effective. In fact, the MCPCNN is a technique that can effectively classify features arranged in the polar coordinate system. A technique using the rubber band straightening transformation, independently developed by Sahnier *et al.* [11], for the detection of masses also employs a similar concept in extracting feature and/or texture in the polar coordinate system. We believe that integration of features and texture values computed at small sectors will be the research trend in mass detection and tumor classification.

VI. CONCLUSION

In the clinical course of detecting masses, mammographers usually evaluate the surrounding background of a radiodense area when an ROI is suspected. In this study, we simulated this fundamental concept with a neural network system (i.e., MCPCNN). In order for the MCPCNN to function, boundary features of the suspicious region in each radial sector were computed. We found that the MCPCNN is capable of analyzing correlated features within the sector and between adjacent sectors, which led to an improvement in detecting mammographic masses.

Through this study, we found that the selected features are somewhat effective in the detection of masses. These features

were "computationally translated" from the qualitative descriptors of BI—RAD. These features can be extended for the improvement of the mass detection, but this task is beyond the scope of this paper. With the preliminary studies shown above, we found the MCPCNN coupling with the proposed training method produced greater results than the conventional neural network. We found that the performances of both neural network systems were improved in Experiment 2. This may have occurred due to the number of training samples that was increased from 54 to 124. In Experiment 2, the A_z value was improved by 0.042 using the MCPCNN, which was higher than the A_z difference of 0.012 obtained by the conventional training method. The results implied that the MCPCNN learned more effectively than the conventional neural network when the number of training cases was increased. With the use of a larger database and advanced texture features proposed by others, it is expected that the performance of MCPCNN should be significantly improved. This paper does not intend to claim the best mass detection system, in comparison to similar systems; but rather its goal is to report a potentially better neural network structure for analyzing a set of mass features.

ACKNOWLEDGMENT

A part of the database, used in the study, was provided by Dr. R. Shah of Brooke Army Medical Center. The LABROC4 and CLABROC programs were written by Dr. C. E. Metz and his colleagues at the University of Chicago.

REFERENCES

- [1] L. Nystrom, L. E. Rutqvist, S. Wall, A. Lindgren, M. Lindqvist, and S. Ryden *et al.*, "Breast cancer screening with mammography: Overview of Swedish randomized trials," *Lancet*, vol. 341, pp. 973–978, 1993.
- [2] S. Shapiro, "Screening-assessment of current studies," *Cancer*, vol. 74, pp. 231–238, 1994.
- [3] L. Tabar, G. Fagerberg, S. Duffy, N. E. Day, A. Gad, and O. Grontoft, "Update of the Swedish two-country program of mammographic screening for breast cancer," *Radiol. Clin. N. Amer.: Breast Imag.—Current Status Future Directions*, vol. 30, pp. 187–210, 1992.
- [4] D. Brzakovic, X. M. Luo, and P. Brzakovic, "An approach to automated detection of tumors in mammograms," *IEEE Trans. Med. Imag.*, vol. 9, p. 233, Sept. 1990.
- [5] R. Zwiggelaar, T. C. Parr, J. E. Schumm, I. W. Hutt, C. J. Taylor, S. M. Astley, and C. R. M. Boggis, "Model-based detection of spiculated lesions in mammograms," *Med. Image Anal.*, vol. 3, no. 1, pp. 39–62, 1999.
- [6] N. Petrick, H. P. Chan, D. Wei, B. Sahiner, M. A. Helvie, and D. D. Adler, "Automated detection of breast masses on mammograms using adaptive contrast enhancement and texture classification," *Med. Phys.*, vol. 23, no. 10, pp. 1685–1696, 1996.
- [7] B. Sahiner, H. P. Chan, N. Petrick, D. Wei, M. A. Helvie, D. D. Adler, and M. M. Goodsitt, "Classification of mass and normal breast tissues: A convolution neural network classifier with spatial domain and texture images," *IEEE Trans. Med. Imag.*, vol. 15, pp. 598–610, Oct. 1996.
- [8] D. Wei, H. P. Chan, M. A. Helvie, B. Sahiner, N. Petrick, D. D. Adler, and M. M. Goodsitt, "Classification of mass and normal breast tissue on digital mammograms: Multiresolution texture analysis," *Med. Phys.*, vol. 25, no. 4, pp. 516–526, 1998.
- [9] L. Hadjiiski, B. Sahiner, H. P. Chan, N. Petrick, and M. A. Helvie, "Classification of malignant and benign masses based on hybrid ART2LDA approach," *IEEE Trans. Med. Imag.*, vol. 18, pp. 1178–1187, Dec. 1999.
- [10] H. Kobatake, M. Murakami, H. Takeo, and S. Nawano, "Computerized detection of malignant tumors on digital mammograms," *IEEE Trans. Med. Imag.*, vol. 18, pp. 369–378, May 1999.
- [11] B. Sahiner, H. P. Chan, N. Petrick, M. A. Helvie, and M. M. Goodsitt, "Computerized characterization of masses on mammograms: The rubber band straightening transform and textures analysis," *Med. Phys.*, vol. 25, no. 4, pp. 516–526, 1998.
- [12] M. A. Kupinski and M. L. Giger, "Automated seeded lesion segmentation on digital mammograms," *IEEE Trans. Med. Imag.*, vol. 17, pp. 510–517, Aug. 1998.
- [13] D. D. Adler, "Breast Masses: Differential Diagnosis," in *ARRS Categorical Course Syllabus on Breast Imaging*, S. A. Feig, Ed. Reston, VA: Amer. Roent. Ray Soc., 1988, p. 31.
- [14] M. J. Homer, "Imaging features and management of characteristically benign and probably benign breast lesions," *Radiol. Clin. N. Amer.*, vol. 25, p. 939, 1987.
- [15] S. Pohlman, K. A. Powell, N. A. Obuchowski, W. A. Chilcote, and S. Grundfest-Broniatowski, "Quantitative classification of breast tumors in digitized mammograms," *Med. Phys.*, vol. 23, no. 8, pp. 1337–1345, 1996.
- [16] M. Moskowicz, "Circumscribed lesions of the breast," in *Diagnostic Categorical Course in Breast Imaging*, M. Moskowicz, Ed. Oak Brook, IL: Radiol. Soc. N. Amer., 1986, p. 31.
- [17] E. A. Sickles, "The rule of multiplicity and the developing density sign," in *ARRS Categorical Course Syllabus on Breast Imaging*, S. A. Feig, Ed. Reston, VA: Amer. Roent. Ray Soc., 1988, p. 177.
- [18] H. Li, Y. Wang, K.-J. R. Liu, S.-C. B. Lo, and M. T. Freedman, "Computerized radiographic mass detection—Part I: Lesion site selection by morphological enhancement and contextual segmentation," *IEEE Trans. Med. Imag.*, pp. 289–301, Apr. 2001.
- [19] —, "Computerized radiographic mass detection—Part II: Decision support by featured database visualization and modular neural networks," *IEEE Trans. Med. Imag.*, pp. 302–313, Apr. 2001.
- [20] *Breast Imaging—Reporting and Data System*. Reston, VA: Ame. Coll. Radiol., 1993.
- [21] J. Suckling, J. Parker, D. Dance, S. Astley, I. Hutt, C. Boggis, I. Ricketts, E. Stamatakis, N. Cerneaz, S. Kok, P. Taylor, D. Betal, and J. Savage, "The mammographic images analysis society digital mammogram database," in *Excerpta Medica*, ser. Int. Congr., 1994, vol. 1069, (e-mail for inquiry: mias@sv1.smb.man.ac.uk.), pp. 375–378.
- [22] S. Haykin, *Neural Networks: A Comprehensive Foundation*, 2nd ed. Englewood Cliffs, NJ: Prentice-Hall., 1999.
- [23] D. E. Rumelhart, G. E. Hinton, and R. J. Williams, "Learning internal representation by error propagation," in *Parallel Distributed Processing: Explorations in the Microstructure of Cognition*, D. E. Rumelhart and J. L. McClelland, Eds. Cambridge, MA: M.I.T. Press, 1986, vol. 1, Foundation, ch. 8, pp. 318–362.
- [24] S.-C. B. Lo, S. L. Lou, J. S. Lin, M. T. Freedman, M. V. Chien, and S. K. Mun, "Artificial convolution neural network techniques and applications to lung nodule detection," *IEEE Trans. Med. Imag.*, vol. 14, pp. 711–718, Dec. 1995.
- [25] S.-C. B. Lo, H. P. Chan, J. S. Lin, H. Li, M. T. Freedman, and S. K. Mun, "Artificial convolution neural network for medical image pattern recognition," *Neural Networks*, vol. 8, no. 7/8, pp. 1201–1214, 1995.
- [26] H. P. Chan, S.-C. B. Lo, B. Sahiner, K. L. Lam, and M. A. Helvie, "Computer-aided diagnosis of mammographic microcalcifications: Pattern recognition with an artificial neural network," *Med. Phys.*, vol. 24, no. 10, pp. 1555–1567, 1995.
- [27] Y. Wu, K. Doi, M. L. Giger, and R. M. Nishikawa, "Computerized detection of clustered microcalcifications in digital mammograms: Applications of artificial neural networks," *Med. Phys.*, vol. 19, pp. 555–560, 1992.
- [28] Y. Wu, M. T. Freedman, S.-C. B. Lo, R. A. Zuurbier, A. Hasegawa, and S. K. Mun, "Classification of microcalcifications in radiographs of pathological specimen for the diagnosis of breast cancer," *Acad. Radiol.*, vol. 2, pp. 199–204, 1995.
- [29] C. E. Metz, B. A. Herman, and J. H. Shen, "Maximum likelihood estimation of receiver operating characteristic (ROC) curves from continuously-distributed data," *Statist. Med.*, vol. 17, pp. 1033–1053, 1998.
- [30] K. Fukunaga and R. R. Hayes, "Effects of sample size in classifier design," *IEEE Trans. Pattern Anal. Machine Intell.*, pp. 873–885, Aug. 1989.
- [31] C. E. Metz, P.-L. Wang, and H. B. Kronman, "A new approach for testing the significance of differences between ROC curves measured from correlated data," in *Information Processing in Medical Imaging*, F. Deconinck, Ed. The Hague, The Netherlands: Martinus Nijhoff, 1984, vol. PAMI-II, pp. 432–445.

AUTOMATIC SEGMENTATION OF MAMMOGRAPHIC MASSES USING FUZZY SHADOW AND MAXIMUM-LIKELIHOOD ANALYSIS

Lisa Kinnard^{a,b,c}, Shih-Chung B. Lo^a, Paul Wang^c, Matthew T. Freedman^a, Mohamed Chouikha^b

^aISIS Center, Dept. of Radiology, Georgetown University Medical Center, Washington, D.C., USA

^bDept. of Electrical Engineering, Howard University, Washington, D.C., USA

^cBiomedical NMR Laboratory, Department of Radiology, Howard University, Washington, D.C., USA

ABSTRACT

This study attempted to accurately segment tumors in mammograms. Although this task is considered to be a preprocessing step in a computer analysis program, it plays an important role for further analysis of breast lesions. The region of interest (ROI) was segmented using the pixel aggregation and region growing techniques combined with maximum likelihood analysis. A fast segmentation algorithm has been developed to facilitate the segmentation process. The algorithm repetitively sweeps the ROI horizontally and vertically to aggregate the pixels that have intensities higher than a threshold. The ROI is then fuzzified by the Gaussian envelope. With each segmented region for a given threshold step in the original ROI, the likelihood function is computed and is comprised of probability density functions inside and outside of the fuzzified ROI. We have implemented this method to test on 90 mammograms. We found the segmented region with the maximum likelihood corresponds to the body of tumor. However, the segmented region with the maximum change of likelihood corresponds to the tumor and its extended margin.

INTRODUCTION

The goal of breast mass segmentation is to separate suspected masses from surrounding tissue as effectively as possible. While it is a pre-processing step of Computer Assisted Diagnosis (CAD_x) it is extremely important in the diagnostic process, because a major characteristic used to separate malignant and benign tumors is shape [1, 12]. Over the years researchers have used many methods to segment masses in mammograms. Petrick [8] et al. used a filtering method called the Density Weighted Contrast Enhancement (DWCE) method. Karssemeijer and te Brake implemented a discrete dynamic contour model [1]. Li et al. developed a competitive classification strategy, which uses a combined soft and hard classification method for deciding if segmented regions are true or false positives. Furthermore, many researchers have implemented methods based on pixel aggregation [3, 5, 7, 9]. A major issue faced by CAD_x researchers is the ability to properly obtain the boundaries of masses because these boundaries are often obscured by surrounding breast tissue. While benign masses can be easily detected due to their well-defined boundaries, the borders of malignant tumors often blend into surrounding tissue, making it exceedingly difficult to properly segment them as effectively as possible. We have developed a maximum likelihood method [3] and have added a component to not only segment the tumor body, but to segment the extended tumor borders as well.

2. METHODS

The next several sections will describe the database, as well as provide the theoretical background used to develop our algorithm.

2.1. Database

The image samples were chosen from several databases compiled by the ISIS Center of the Georgetown University Radiology Department as well as the University of South Florida's (USF) Digital Database for Screening Mammography [2]. They are a mixture of "obvious" cases and "not obvious" cases. The "obvious" cases contain tumors that are easily identifiable as malignant or benign while the "not obvious" cases are those that radiologists find difficult to observe and/or classify. Forty malignant and forty benign tumors were tested during this experiment. The Georgetown University films were scanned at a resolution of 100 μ m while the USF films were scanned at 43.5 and 50 μ m's. We compensated for this discrepancy in resolution by reducing the USF images to half their normal sizes. Hence, the original test images for this study all contain 12 bits per pixel with approximately 100 μ m pixel size.

2.2. Pixel Aggregation and Region Growing

Pixel aggregation is an automated segmentation method in which the region of interest begins as a single pixel (seed point) and grows based on surrounding pixels with similar properties, e.g., grayscale level or texture [4, 11]. Typically, the seed is located at somewhere in the center region with the highest intensity in the suspected lesion. It is a commonly used method [7, 9, 10] due to its simplicity and accuracy. The next 4-neighboring pixel is checked for similarity so that the region can grow. Our algorithm checks the 4-neighbors of the seed pixel and its grown pixels uses a graylevel threshold. The threshold was used as a similarity criterion. The algorithm repetitively sweeps the ROI horizontally and vertically to aggregate the pixels that have intensities higher than a threshold. Sweeping the neighboring pixels in the alternate direction is a fast region aggregation algorithm that we have recently developed. The iteration ends when no more pixels are acquired in the sweeping step (see Figure 1). The segmented region can be grown by repeating the same method with a lower threshold value. Based on these segmented regions, we can evaluate the regions and region changes with respect to the threshold values. We do not recommend using the 8-neighbor connectivity method for it may

invade the surrounding tissue at the critical threshold to be discussed below.

At the conclusion of the each region segmentation in the sweeping process, there were several holes located inside the detected ROI. We used a chain code to detect the boundaries of these holes and then fill them using a threshold criterion. The output images of the above computer procedures are then used as templates (S_i) for the maximum likelihood analysis.

2.3. Fuzzy Shadow and Maximum Likelihood Analysis

By using the same seed point with multiple intensity threshold values, we obtained between 20 and 50 segmentation partitions per lesion. Kupinski and Giger proposed a maximum-likelihood based method to choose the best partition [3]. However, their method did not completely address the issue in identifying the tumor margin. Since the mammographic masses may or may not have their extended boundaries, it is important to separate the region of tumor body from its extended region. We adapt Kupinski and Giger's point in composing the ROI with a Gaussian envelope, which further fuzzies the tumor margin. With each segmented region for a given threshold step in the original ROI, the likelihood function is computed so that it consists of probability density functions inside and outside of the fuzzified ROI.

The maximum likelihood method is based upon the probability density function (pdf), which for an image, is the histogram. Given a template S_i , which was described in section 2.1.1. we can model the image's pixel probabilities in the following way:

$$p(f(x,y)|S_i, \sigma_i^2) = \begin{cases} \text{Hist}(f(x,y)) \exp\left[-(x^2 + y^2)/(2\sigma_i^2)\right] & (x,y) \in S_i \\ \text{Hist}(f(x,y)) & (x,y) \notin S_i \end{cases} \quad (1)$$

where Hist represents the histogram function. A Gaussian envelope with variance σ_i^2 centered at the seed point gray level was employed. The Gaussian envelope is a special case of the proposed fuzzy shadow. The size and standard deviation (σ_1) used in the experiment were 1400 and 160 pixels, respectively. These values were found experimentally, however, there are more statistical methods found in literature. Equation (2) defines the likelihood that a tumor is contained in the segmented region S_i :

$$p(I|S_i, \sigma_i^2) = \prod_{(x,y) \in L_i} p(f(x,y)|S_i, \sigma_i^2) \quad (2)$$

Equation (2) was implemented by summing the log of the probabilities of all pixel values inside S_i (segmented region) and outside S_i (background). Note that S_i is the segmented region based on the original ROI, not the fuzzified ROI. The likelihood for various partitions was then analyzed to obtain the final segmentation. The partition is chosen for the body of the tumor based on the following criterion:

$$p(I|S_{\text{body}}, \sigma_i^2) = \arg\max p(f(x,y)|S_i, \sigma_i^2) \quad (3)$$

Based on our investigation, we further define that the step before maximum changes of likelihood value is the tumor margin:

$$p(I|S_{\text{margin}}, \sigma_i^2) = \arg\max \left[\frac{d p(f(x,y)|S_i, \sigma_i^2)}{d i} \right] \quad (4)$$

3. RESULTS

The following graphics are experimental results for one patient. Figure 1 shows the a portion of the pixel aggregation process, Figure 2, is the plot produced by summing all probability values inside and outside L_i for various intensities, and Figure 3 shows the original image followed by the tumor body image and the extended tumor body image.

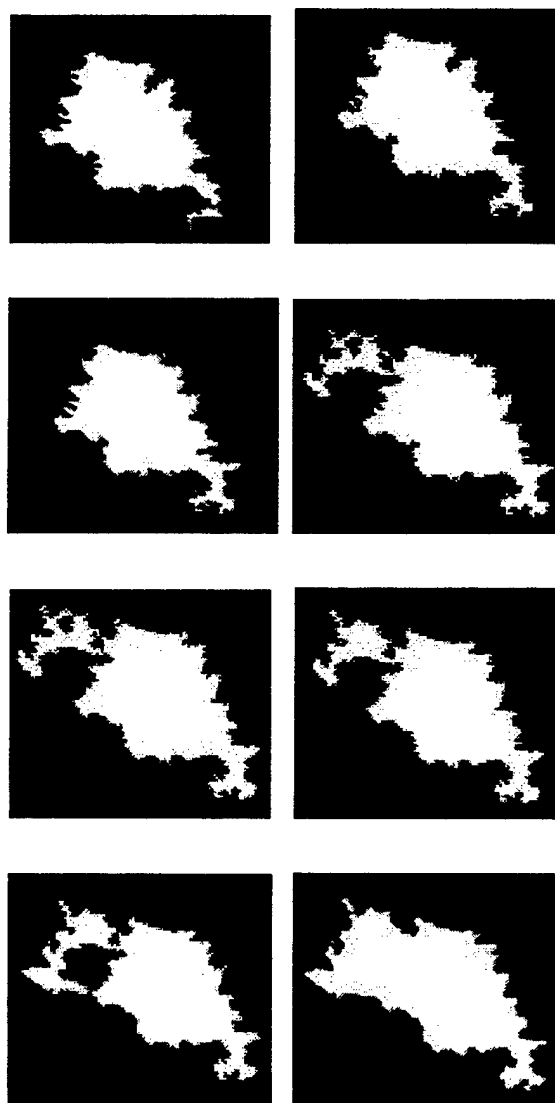


Figure 1 – Several iterations of the pixel aggregation process

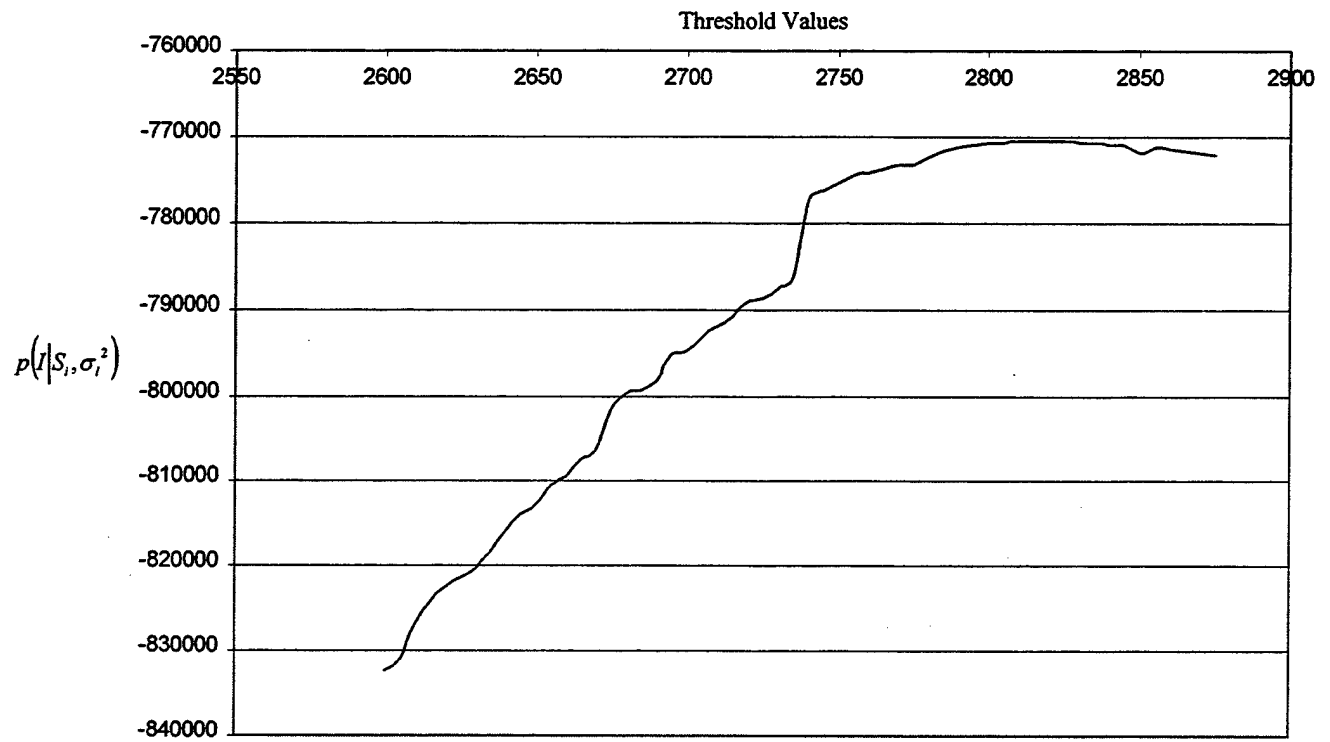


Figure 2 – Plot of the sum of the logarithm values for various image intensities

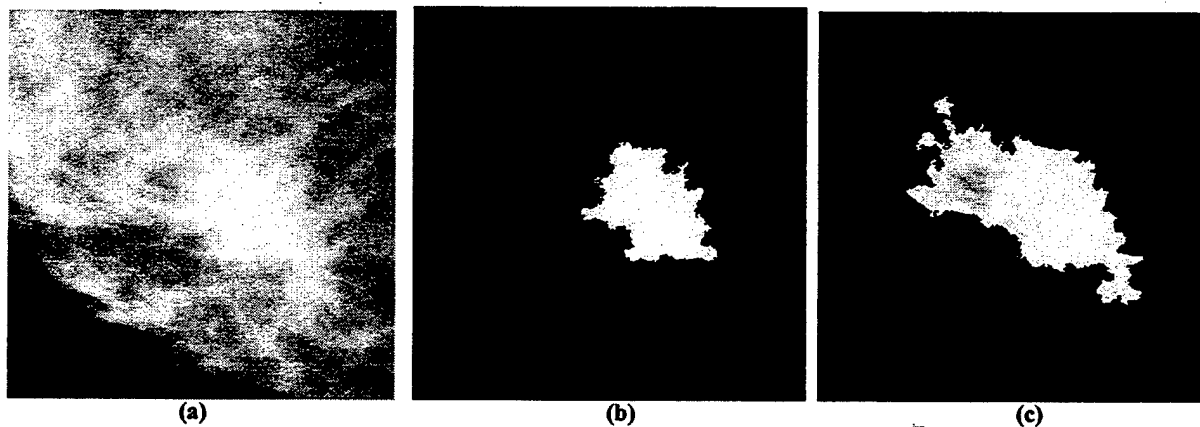


Figure 3 – (a) original image, (b) image of tumor body, (c) image of tumor body with extended borders

Instead of using the Gaussian enveloped image for the segmented region, we use the original image for each step of region growing in this study, simply because Gaussian enveloped image distorts the original intensities and boundaries. However, it facilitates the likelihood analysis by fuzzifying the tumor region. We found that this partition effectively segmented the tumor body, but often did not include the borders. We performed a study prior to the one described in this paper on 30 mammograms and discovered that the best segmentation result including the tumor margin occurs at the steepest ascent location on the plot of $p(I|S, \sigma_i^2)$. In this particular study, the

maximum value on the plot of $p(I|S, \sigma_i^2)$ corresponded to the tumor body segmentation result (see Figure 3). Figure 2 shows that this sharp increase occurs at intensity 2745, therefore it can be inferred that the best segmentation result is produced when the seed point intensity is approximately 2745. The maximum value on the curve occurs at intensity 2815, therefore, when the tumor body segmentation result was found for this particular intensity value.

We discovered that this method is particularly helpful when the masses have ill-defined borders. In most cases in which the mass boundary is ill-defined, the probability curve increases in a steady fashion, while the cases in which the mass boundary is well-defined, the steep ascent location is very abrupt. In some cases we found that this ascent location to be so abrupt, that it could be compared to a step function.

4. DISCUSSION AND CONCLUSION

We have developed a mass segmentation method that is capable of delineating a mass body, as well as its borders. We believe that it outperforms traditional region growing techniques. Traditional region growing without the use of a quantitative method can introduce a great deal of subjectivity because given a large number of segmentation results, what is perceived to be the best one can vary greatly from one researcher to another. By analyzing the likelihood of the segmented regions, it is rational to identify that the maximum likelihood of the segmented regions corresponds to the tumor body and the maximum likelihood change of the segmented regions corresponds to the tumor margin. For the latter, we would like to indicate that when the segmented region significantly increases with the threshold increment, the likelihood value would also significantly change. In most cases, the significant change of the segmented region implies that the tumor margin grows and invades the surrounding tissues because their intensity difference is usually very small.

6. REFERENCES

[1] Brake GM te, Karssemeijer N, Segmentation of suspicious densities in digital mammograms, *Medical Physics*, 2001, vol. 28, no. 2, pp. 259-266.

[2] Heath M, Bowyer KW, Kopans D et al, "Current status of the Digital Database for Screening Mammography," *Digital Mammography*, Kluwer Academic Publishers, 1998, pp. 457-460.

[3] Kupinski MA, Giger ML, Automated Seeded Lesion Segmentation on Digital Mammograms, *IEEE Transactions on Medical Imaging*, 1998, vol. 17, no. 4, pp. 510-517.

[4] Gonzalez RC, Woods RE, *Digital Image Processing* Reading, MA: Addison Wesley, 1992.

[5] Li H, Wang Y, Liu KJR, Lo S-C, Freedman MT, Computerized Radiographic Mass Detection - Part I: Lesion Site Selection by Morphological Enhancement and Contextual Segmentation, *IEEE Transactions on Medical Imaging*, 2001, vol. 20, no. 4, pp. 289-301.

[6] Li L, Zheng Y, Zhang L, Clark R, False-positive reduction in CAD mass detection using a competitive classification strategy, *Medical Physics*, 2001, Vol. 28, no. 2, pp. 250-258.

[7] Mendez AJ, Tahoces PG, Lado MJ, Souto M., Vidal JJ, Computer-aided diagnosis: Automatic detection of malignant masses in digitized mammograms, *Medical Physics*, 1998, vol. 25, no. 6, pp. 957-964.

[8] Petrick N, Chan H-P, Sahiner B, Wei D, An Adaptive Density-Weighted Contrast Enhancement Filter for Mammographic Breast Mass Detection, *IEEE Transactions on Medical Imaging*, 1996, vol. 15, no. 1, pp. 59-67.

[9] Pohlman S, Powell KA, Obuchowski NA, Chilcote WA, Grundfest-Broniatowski S, "Quantitative classification of breast tumors in digitized mammograms", *Medical Physics*, 1996, vol. 23, no. 8, pp. 1336-1345.

[10] Sahiner B, Chan HP, Wei D, Petrick N, Helvie MA, Adler DD, Goodsit MM, Image feature selection by a genetic algorithm: Application to classification of mass and normal breast tissue, *Medical Physics*, 1996, vol. 23, no. 10, pp. 1671-1684.

[11] Sonka M, Hlavac V, Boyle R, "Image Processing, Analysis and Machine Vision".

[12] Tabar L, Dean P. *Teaching Atlas of Mammography*, Georg Thieme Verlag, Stuttgart, Germany, 1983, 1985.

7. ACKNOWLEDGMENTS

Kinnard and Wang were supported in part by Army grant DAMD17-96-1-6254. Kinnard, Lo, Wang, Freedman, and Chouikha were supported in part by Army grant DAMD17-00-1-0627.

Separation of Malignant and Benign Masses Using Image and Segmentation Features

Lisa Kinnard^{a,b}, Shih-Chung B. Lo^a, Paul Wang^c, Matthew T. Freedman^a, Mohamed Chouikha^b

^aISIS Center, Dept. of Radiology, Georgetown University Medical Center, Washington, D.C.

^bDepartment of Electrical Engineering, Howard University, Washington, D.C.

^cBiomedical NMR Laboratory, Department of Radiology, Howard University, Washington, D.C.

ABSTRACT

The purpose of this study is to investigate the efficacy of image features versus likelihood features of tumor boundaries for differentiating benign and malignant tumors and to compare the effectiveness of two neural networks in the classification study: (1) circular processing-based neural network and (2) conventional Multilayer Perceptron (MLP). The segmentation method used is an adaptive region growing technique coupled with a fuzzy shadow approach and maximum likelihood analyzer. Intensity, shape, texture, and likelihood features were calculated for the extracted Region of Interest (ROI). We performed these studies: experiment number 1 utilized image features used as inputs and the MLP for classification, experiment number 2 utilized image features used as inputs and the neural net with circular processing for classification, and experiment number 3 used likelihood values as inputs and the MLP for classification. The experiments were validated using an ROC methodology. We have tested these methods on 51 mammograms using a leave-one-case-out experiment (i.e., Jackknife procedure). The A_z values for the four experiments were as follows: 0.66 in experiment number 1, 0.71 in experiment number 2, and 0.84 in experiment number 3.

Keywords: Computer-assisted diagnosis, breast cancer, convolution neural networks, feature extraction

1. INTRODUCTION

Many studies have investigated the efficacy of various features used in Computer-Assisted Diagnostic (CAD_x) systems. Sahiner et al.¹³ used texture and morphological features and used a genetic algorithm to select the best image features. In a study used to differentiate dense tissue from fatty tissue, Byng et al.¹ used fractal dimension and regional skewness as features. Qian et al.¹² calculated circularity, normalized deviation of radial length, intensity variation, mean intensity difference, and the mean gradient of region boundary. Wei et al.¹⁶ calculated the following eight texture features from the co-occurrence matrix: correlation, energy, entropy, inertia, inverse difference moment, sum average, sum entropy, and difference entropy. In a later study, Sahiner et al.¹⁵ calculated a Fourier descriptor, convexity, rectangularity, perimeter, Normalized Radial Length (NRL) mean, contrast, NRL entropy, circularity, NRL area ratio, NRL standard deviation, NRL zero crossing count, perimeter-to-area ratio, and area. These and other studies have been successful in finding features that are effective in separating from benign features, however, our study uses traditional features as well as segmentation features as inputs to two different classifiers.

In the United States, breast cancer accounts for one-third of all cancer diagnoses among women and it has the second highest mortality rate of all cancer deaths⁴. In various studies it has been shown that only 13% - 29% of suspicious lesions were determined to be malignant^{11, 13, 17} which indicates that there are high false positive rates for biopsied breast lesions. A higher predictive rate is anticipated by combining the mammographer's interpretation and the computer analysis. This could be of great clinical value because a lower amount of false positives in breast biopsies would reduce anxiety among patients and their families. Other studies show that 7.6-14% of the patients have mammograms that produce false negative diagnoses^{3, 8}. Alternatively, a CAD_x system can serve as a clinical tool for the radiologist and consequently lower the rate of missed breast cancer.

2. METHODOLOGY

The next several sections will describe the database, as well as provide the theoretical background used to develop the CAD_x experiment.

2.1 Database

The image samples were chosen from several databases compiled by the ISIS Center of the Georgetown University Radiology Department as well as the University of South Florida's (USF) Digital Database for Screening Mammography⁴. Twenty-eight malignant and twenty-three benign tumors were tested during this experiment.

2.2 Maximum Likelihood Segmentation Method

The segmentation method used in this study is an adaptive region growing technique coupled with a fuzzy shadow approach and maximum likelihood analyzer. The region growing technique aggregates surrounding pixels with similar properties, e.g., grayscale level. It is a commonly used method due to its simplicity and accuracy. The intensity threshold is usually used as a similarity criterion. We used the highest intensity as the seed point with multiple intensity threshold values and decreased the gray level in successive steps. This method by itself generated a sequence of contour on the mass; however, the computer did not have the ability to determine the boundaries interfered by other tissues and to choose the proper partition corresponding to the experts' perception. A fuzzy operator and a maximum-likelihood component were therefore added to the region-growing algorithm. The likelihood function is comprised of the likelihood of the composite probabilities for probability density functions (PDF's) inside ($p(S_i|pdf_i)$) and outside ($p(S_i|ROI)$) a given contour (see example contour in Figure 1)².

$$\text{Log}(P_i) = \log(p(S_i|pdf_i)) + \log(p(S_i|ROI)) \quad (1)$$

The subscript i represents the thresholding step, or, intensity value used to produce a given contour. The area inside the contour is the original ROI, which has been multiplied by a fuzzy shadow, whereas the area outside the contour is the original ROI. The likelihood that the contour represents the mass's extended borders is determined by assessing the maximum change of the likelihood function^{5,6}:

$$\arg \max \frac{d(\log(P_i))}{di} \quad (2)$$

To summarize, the best contour is determined by locating the steepest jump in likelihood values, i.e., the intensity corresponding to this location will produce the best contour.

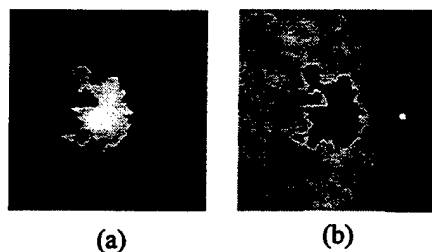


Figure 1: (a) ROI used to calculate $p(S_m|pdf_i)$. (b) ROI used to calculate $p(S_m|ROI)$ where m is the m^{th} contour corresponding to the maximum value of likelihood function indicated in eq. (2).

2.3 Feature Calculation

The features used to separate the malignant and benign masses were a combination of 18 statistical descriptors along with the likelihood features. The features have been separated into global features and sector features, where global features are those for which one value per mass is calculated. Sector features are those features calculated on the 10° ROI as it was divided into 10° sectors in the polar coordinate system (see Figure 2); therefore, each mass contained 36 sectors.

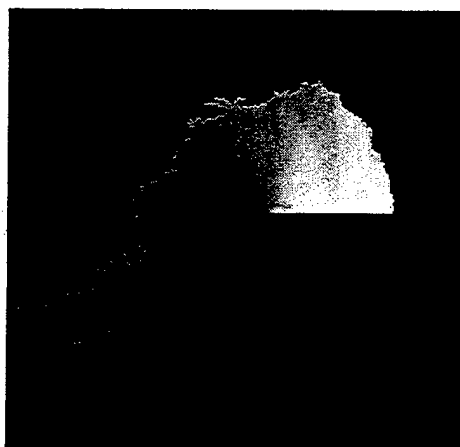


Figure 2: Sample map used to calculate sector features

In this study, three sets of features were used. One set of features is related to the use of the likelihood function curve which will be discussed in section 3. The other sets of features are as follows:

Global Features: skewness, kurtosis, circularity, compactness, and mass perimeter.

Local Features: mean intensity value, contrast, standard deviation inside the sector, sector area, deviation of the normalized radial length, radial length, roughness, energy, inertia, entropy, inverse difference moment, and difference entropy.

3. EXPERIMENTS

In experiment 1 the input features consisted of 6 global image features combined with 12×36 sector image features to yield a total of 438 features. The classifier used for this experiment was a MLP neural network. It contained 18 hidden nodes and one output. Experiment 2 used the same image input features as those used in experiment 1, yet the classifier used for this experiment was the MCPCNN. The MCPCNN also contained 18 hidden nodes and one output. The neural networks were both tested and trained using the jackknife method. In experiment 3 the input values consisted of likelihood values that were extracted from the segmentation likelihood functions (see Figures 5, 6). The classifier used in this experiment was a MLP with 15 hidden nodes and one output. The neural network for this experiment was also tested and trained using the jackknife method. The results were analyzed using the LABROC4 analysis tool¹⁰. The experiments are summarized in Table 1.

4. RESULTS

The following table (Table 1) is a summary of the results achieved by the two classifiers used in the experiments described in section 2 of this paper. The corresponding ROC curves are shown in Figure 4. Two likelihood functions (features used in Experiment 3) along with their segmentation results (one malignant and one benign) are shown in Figures 5 and 6.

Table 1: Summary of Classification Results

Experiment	Features	Neural Network	A_z values
1	Image Features	MLP	0.66
2	Image Features	MCPCNN	0.71
3	ML-curve as features	MLP	0.84

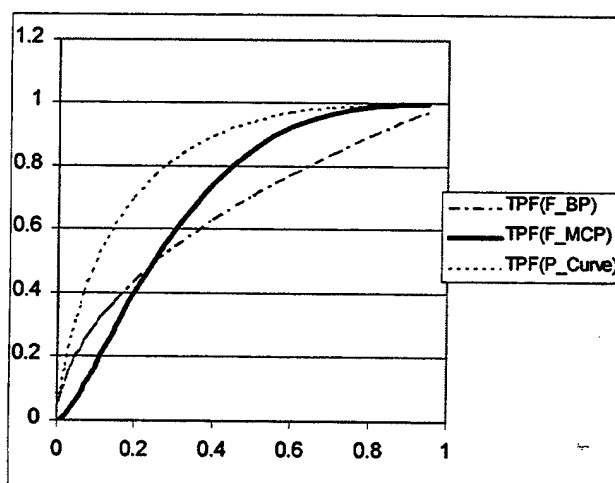


Figure 4: ROC Results (TPF: True Positive Fraction, F_BP: Experiment 1, F_MCP: Experiment 2, P_Curve: Experiment 3)

(Abstract: ISMRM workshop on Dynamic Spectroscopy and Measurements of Physiology, Metabolism, and Function, 6-8 September 2003, Orlando, FL)

A Pharmacokinetic Study of Trifluoperazine Crossing Blood-Brain-Barrier Due to P-glycoprotein Modulation

¹Paul C Wang, ²Adorjan Aszalos, ¹Ercheng Li, ¹Renshu Zhang, ¹Huafu Song

¹Department of Radiology, Howard University, Washington, DC

²National Cancer Institute, Bethesda, MD, and Food and Drug Administration, College Park, MD

INTRODUCTION Elderly patients and patients with cancer are often treated with combination therapy such as depression, and cardiopulmonary diseases in addition to for their primary symptoms. The potential for drug-drug interaction under these conditions is high. Such interactions may cause changes in the pharmacokinetics, especially for drugs with narrow therapeutic indices (1, 2). These changes can alter efficacy and toxicity of the administered drugs. Drug-drug interactions may occur due to common metabolic pathways, but also due to interference at the P-glycoprotein (Pgp) level. Pgp, which is a nonspecific transport protein, is expressed constitutively at the blood-brain-barrier (BBB), intestine, kidney, and liver (3). Interaction at the blood-brain barrier may occur if Pgp is blocked by a drug and a concomitantly administered second drug, which would not penetrate brain if administered singly, can then penetrate the brain freely (4,5). The potential for drug-drug interactions is not routinely studied at the Pgp level during drug development. Its presence is assumed only after unexpected clinical symptoms. In this study, we have used a dynamic NMR method based on detection of a fluorinated drug, trifluoperazine (TFP), in the brain, in combinations with an immune suppressor, cyclosporin A to demonstrate the drug penetration through the blood-brain-barrier due to Pgp modulation.

METHODS Sprague-Dawley rats, weight 200 g, were used. The rats were anesthetized by i.p. injection of sodium pentobarbital 40 mg/kg. After anesthesia, a Pgp modulator cyclosporin A (15 mg/kg) was administered through the tail vein. Fifteen minute later, trifluoperazine (25 mg/kg) was injected. For detection of trifluoperazine in the brain, ¹⁹F NMR studies were performed using 4.7 T, 33 cm horizontal bore NMR machine. A 22 mm x 17 mm surface coil was positioned immediately adjacent to the rat skull. A small bulb containing trifluoroacetic acid was used as an extern reference. After shimming and tuning, a series of 10 minutes spectra were obtained. The repetition time was one second.

RESULTS In Figure 1, the spectrum A shows a control, in which only TFP was administered. The spectrum B shows an increase amount of TFP crossing BBB after co-administering a Pgp modulator, cyclosporin A. This demonstrates the synergistic effect of cyclosporin A with TFP. Figure 2 shows nine continuous ¹⁹F spectra from the rat brain after administering cyclosporin A and TFP. Each spectrum takes 10 minutes. The first spectrum in the Figure 2 is taken before TFP injection as a baseline. For the second 10 minutes during the TFP injection, there is an increase of fluorine signal. The following spectra 3-9 show the accumulation of TFP and gradual decreasing of fluorine signal due to metabolism.

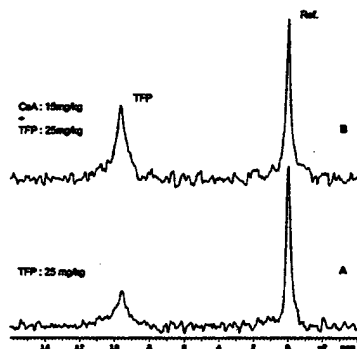


Figure 1

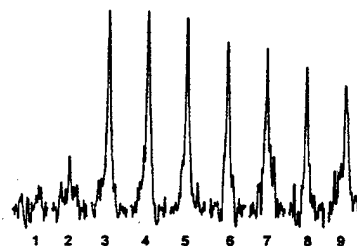


Figure 2

DISCUSSION This experiment has demonstrated that concomitantly administered a Pgp modulator enhanced TFP, an antipsychotic drug, crossing BBB in vivo. It also demonstrated the pharmacokinetics of TFP accumulation in the brain. The pharmacology of this noninvasive model for realizing opening of the BBB in case of possible drug-drug interaction at the Pgp level was based on drug know to modulate Pgp and on the drug which can be detected by ¹⁹F NMR spectroscopy. In case of polypharmacy, like with elderly or cancer patients, drug-drug interaction is not always understood. The noninvasive dynamic NMR spectroscopy study of drug-drug interactions can be a very useful tool in drug development.

REFERENCES

1. Balis FM, Clin. Pharmacokin., 11, 223-235, 1986
2. Ibrahim S, Peggins J, Knapp A, Licht T, Aszalos A, Anticancer Res., 21, 847-856, 2001
3. Gottesman MM, Fojo T and Bates SE, Nature Reviews, 2, 48-58, 2002
4. Schinkel A, Wagenaar F, Mol C and Van Deemter L, J. Clin. Invest., 97,2517-2524, 1996
5. Tatsura T, Naito M, Ohhara T, Sugawara I and Tsuruo T, J. Biol. Chem., 267,20383-20391, 1992